

Enpolarization and depolarization of light scattered from chromatic complex media

G. Soriano,* M. Zerrad, and C. Amra

Aix-Marseille Université, CNRS, Centrale Marseille, Institut Fresnel, UMR 7249, 13013
Marseille, France

[*gabriel.soriano@fresnel.fr](mailto:gabriel.soriano@fresnel.fr)

Abstract: Influence of the variations of the scattering properties of a disordered medium with respect to frequency on the polarization of scattered light is investigated. We focus on the strongly scattering regime with the sum of random phasors scattering model that is extended to chromatic media and made frequency-sensitive. It is numerically shown how the scattered polarization depends on the incident polarization and the incident light bandwidth to scattering coefficients chromatic length ratio. Under the presented approach, both phenomena of depolarization and enpolarization of light appear unified.

© 2014 Optical Society of America

OCIS codes: (030.6600) Statistical optics; (030.1640) Coherence; (290.5855) Scattering, polarization; (030.6140) Speckle; (260.5430) Polarization.

References and links

1. R. Martínez-Herrero, P. M. Mejias, and G. Piquero, *Characterization of partially polarized light fields* (Springer, 2009), vol. 147.
2. G. Gbur and T. Visser, “The structure of partially coherent fields,” *Prog. Opt.* **55**, 285 (2011).
3. B. DeBoo, J. Sasian, and R. Chipman, “Degree of polarization surfaces and maps for analysis of depolarization,” *Opt. Express* **12**, 4941–4958 (2004).
4. A. Pierangelo, A. Benali, M.-R. Antonelli, T. Novikova, P. Validire, B. Gayet, and A. De Martino, “Ex-vivo characterization of human colon cancer by mueller polarimetric imaging,” *Opt. Express* **19**, 1582–1593 (2011).
5. E. Wolf, *Introduction to the Theory of Coherence and Polarization of Light* (Cambridge University Press, 2007).
6. O. Angelsky, S. G. Hanson, C. Y. Zenkova, M. Gorsky, and N. Gorodyska, “On polarization metrology (estimation) of the degree of coherence of optical waves,” *Opt. Express* **17**, 15623–15634 (2009).
7. F. Goudail and A. Bénéière, “Estimation precision of the degree of linear polarization and of the angle of polarization in the presence of different sources of noise,” *Appl. Opt.* **49**, 683–693 (2010).
8. L. Pouget, J. Fade, C. Hamel, and M. Alouini, “Polarimetric imaging beyond the speckle grain scale,” *Appl. Opt.* **51**, 7345–7356 (2012).
9. A. Ghabbach, M. Zerrad, G. Soriano, and C. Amra, “Accurate metrology of polarization curves measured at the speckle size of visible light scattering: surface signatures,” submitted to *Opt. Express*.
10. Z. Tong and O. Korotkova, “Theory of weak scattering of stochastic electromagnetic fields from deterministic and random media,” *Phys. Rev. A* **82**, 033836 (2010).
11. C. Ding, Y. Cai, Y. Zhang, and L. Pan, “Scattering-induced changes in the degree of polarization of a stochastic electromagnetic plane-wave pulse,” *J. Opt. Soc. Am. A* **29**, 1078–1090 (2012).
12. J. Sorrentini, M. Zerrad, G. Soriano, and C. Amra, “Enpolarization of light by scattering media,” *Opt. Express* **19**, 21313–21320 (2011).
13. P. Réfrégier, M. Zerrad, and C. Amra, “Coherence and polarization properties in speckle of totally depolarized light scattered by totally depolarizing media,” *Opt. Lett.* **37**, 2055–2057 (2012).
14. M. Zerrad, G. Soriano, A. Ghabbach, and C. Amra, “Light enpolarization by disordered media under partial polarized illumination: The role of cross-scattering coefficients,” *Opt. Express* **21**, 2787–2794 (2013).
15. G. Soriano, M. Zerrad, and C. Amra, “Mapping the coherence time of far-field speckle scattered by disordered media,” *Opt. Express* **21**, 24191–24200 (2013).

16. J. Ellis, A. Dogariu, S. Ponomarenko, and E. Wolf, "Correlation matrix of a completely polarized, statistically stationary electromagnetic field," *Opt. Lett.* **29**, 1536–1538 (2004).
17. J. Broky and A. Dogariu, "Complex degree of mutual polarization in randomly scattered fields," *Opt. Express* **18**, 20105–20113 (2010).
18. J. Broky and A. Dogariu, "Correlations of polarization in random electro-magnetic fields," *Opt. Express* **19**, 15711–15719 (2011).
19. M. Zerrad, J. Sorrentini, G. Soriano, and C. Amra, "Gradual loss of polarization in light scattered from rough surfaces: Electromagnetic prediction," *Opt. Express* **18**, 15832–15843 (2010).
20. J. Sorrentini, M. Zerrad, and C. Amra, "Statistical signatures of random media and their correlation to polarization properties," *Opt. Lett.* **34**, 2429–2431 (2009).
21. M. Zhang, Z. Li, X. Chen, G. Liang, S. Wang, S. Teng, and C. Cheng, "Evolutions of speckles on rough glass/silver surfaces with film thickness," *Opt. Express* **21**, 8831–8842 (2013).
22. J. Stratton and L. Chu, "Diffraction theory of electromagnetic waves," *Phys. Rev.* **56**, 99–107 (1939).
23. A. Ishimaru, *Wave Propagation and Scattering in Random Media*, an IEEE OUP classic reissue (Wiley, 1999).
24. J. Van Bladel, *Electromagnetic fields* (Wiley-IEEE Press, 2007), vol. 19.
25. A. G. Voronovich, *Wave scattering from rough surfaces* (Springer-Verlag, 1994).
26. J. Goodman, *Speckle phenomena in optics: theory and applications* (Roberts & Co, 2007).
27. W. H. Press, *Numerical recipes in Fortran 77: the art of scientific computing* (Cambridge University, 1992), vol. 1.
28. C. Brosseau, *Fundamentals of polarized light: a statistical optics approach* (Wiley-Blackwell, 1998).
29. L. Mandel and E. Wolf, *Optical coherence and quantum optics* (Cambridge University, 1995).

1. Introduction

Light polarization still remains the focus of numerous works [1, 2] with a broadening range of applications from remote sensing to living diagnostics [3, 4]. A sophisticated formalism was proposed [5] which gathers both polarization and coherence of light, and allows detailed investigation of polarized data. Within this framework, numerous experiments were driven and have shown great agreement with the predictions [6–9].

However despite this successful story, fewer results can be found on light polarization when disordered but deterministic and stationary media are addressed and their scattering patterns analyzed at the speckle size [10, 11]. In particular recent papers have revealed unexpected enpolarization effects [12–14] in light scattered by complex media. Such enpolarization effects were predicted and compared to experiment with great accuracy [12]. Furthermore, numerical and analytical calculations were shown to be in high agreement [13]. In a last step, these enpolarization effects were quantified versus the polarization degree (DoP) of the incident light [14], and statistical distributions of the scattered polarization degree were pointed out for high scattering media. Also, mapping and histograms of the coherence time were predicted for disordered media [15].

All these studies concerned the classical (local and temporal) degree of polarization, but depolarization was also shown to find its origins in a spatial (rather than temporal) average, which motivated additional recent papers gathering electromagnetic optics and statistical optics [16–18]. Indeed scattering patterns may exhibit rapid variations of polarization from one speckle grain to another, and this variation results in a depolarization effect when the receiver aperture collects at least a few speckle grains. Such effects were quantified on the basis of electromagnetic optics, which allowed us to connect the loss of polarization to the microstructure of the scattering samples [19]. Statistics of the speckle patterns were analyzed versus this microstructure [20, 21].

Within this framework it was shown that most effects result from the presence of cross-polarized scattering coefficients which cannot be neglected for strongly scattering media. Indeed these coefficients allow linear combinations of the incident polarization modes to generate each polarization mode of the scattered light, and this is the key to predict the effects of temporal enpolarization or spatial depolarization.

However until now the spectral (wavelength) variations of these coefficients were neglected

within the bandwidth of the incident source. Such assumption is largely justified with laser sources but may fail when larger bandwidths are considered; moreover, depending on the scattering origins and samples microstructure, the chromaticity of the scattering coefficients may be strongly increased. This is the reason why this assumption was abandoned in this paper, which allowed us to revisit the DoP histograms and provide a more complete analysis. Hence new DoP signatures can now be emphasized to characterize either (local) enpolarization or (local) depolarization effects; these signatures vary with the ratio of the incident bandwidth to that of the scattering coefficients. The paper is focused on polarization and temporal coherence ; studied light sources are assumed to exhibit full spatial coherence.

2. The scattering matrix

The theory of electromagnetic wave diffraction [22] and scattering [23] is generally formalized in the frequency domain. The incident field $\vec{\mathcal{E}}_i(\nu)$ is assumed to have a plane wave structure in the region of the disordered medium. With $\hat{\mathbf{r}}_i$ the propagation direction, two independent components of the electric field in the polarization plane normal to $\hat{\mathbf{r}}_i$ form the vector $\vec{\mathcal{E}}_i(\nu)$. The scattered field is detected in far field conditions. Discarding dependency to the distance between the scattering center and the detector, the scattered field is characterized by its scattering amplitude $\vec{\mathcal{E}}_s(\nu)$, a two-components vector. Hence the incident and scattered fields are written as:

$$\vec{\mathcal{E}}_i(\nu) = \begin{bmatrix} \mathcal{E}_{ix}(\nu) \\ \mathcal{E}_{iy}(\nu) \end{bmatrix} \quad \vec{\mathcal{E}}_s(\nu) = \begin{bmatrix} \mathcal{E}_{sx}(\nu) \\ \mathcal{E}_{sy}(\nu) \end{bmatrix} \quad (1)$$

where the subscripts x and y denote different directions for incident and scattered fields.

With the sole assumption that the scattering medium is linear, incident plane wave and scattered field are linked by the so-called scattering matrix $\vec{\Sigma}(\nu)$ [24, chap. 11] (see also [25]).

$$\vec{\mathcal{E}}_s(\nu) = \vec{\Sigma}(\nu)\vec{\mathcal{E}}_i(\nu) \quad (2)$$

The scattering matrix completely characterizes the scattering medium at frequency ν . This complex 2-matrix is a function of the incident and scattering directions $\hat{\mathbf{r}}_i$ and $\hat{\mathbf{r}}_s$. It writes:

$$\vec{\Sigma}(\nu) = \begin{bmatrix} \Sigma_{xx}(\nu) & \Sigma_{xy}(\nu) \\ \Sigma_{yx}(\nu) & \Sigma_{yy}(\nu) \end{bmatrix} \quad (3)$$

with Σ_{xx} and Σ_{yy} the co-polarized coefficients and Σ_{xy} and Σ_{yx} the cross-polarized coefficients.

In this paper, we rely on a simple and versatile heuristics to modelize the scattering matrix: the random phasors sum [26]. It was recently shown that this phenomenological model is relevant for strongly scattering medium, such as an inhomogeneous bulk with high optical index variations or a rough surface with steep slopes or peak to valley heights larger than the wavelength. In accordance with this model, each of the four coefficients of the scattering matrix (3) is modeled by the far field scattered by n^2 random phasors placed on a plane square regular grid with mesh size δ_x . Those phasors are circular complex gaussian random variables of zero mean and equal variance. They are statistically independent, but the scattered field is obtained by interference of their individual fields. An example is given in Fig. 1.

Since the random phasors sum was designed in a quasi-monochromatic context, it shows no dependency to frequency. We extend the model by adding the time dimension to the two-dimensional spatial array of random phasors. n_t is the number of instants and δ_t denotes the regular time step. The scattered field computation is efficiently performed with three-dimensional Fast Fourier Transforms (FFT) on $N = np$ points along each spatial dimension and $N_t = n_t p_t$ points along the time dimension, using zero-padding [27]. With θ the polar angle and φ the

azimuthal angle, scattering directions can be pointed by the two horizontal components of the wavevector

$$\begin{cases} k_x = (\omega_0/c) \sin \theta \cos \varphi \\ k_y = (\omega_0/c) \sin \theta \sin \varphi \end{cases} \quad (4)$$

Spatially, the scattered field is estimated on a regular grid in the (k_x, k_y) plane with a mesh size $\delta_k = \frac{2\pi}{N\delta_x}$. Each direction $(k_x = i\delta_k, k_y = j\delta_k)$ on this grid is parametered by two integer numbers (i, j) in the range $[1 - N/2 : N/2]$, and corresponds to a pixel on the maps of forthcoming figures. The covered region includes n^2 speckle grains, with p^2 pixels per grain. This region

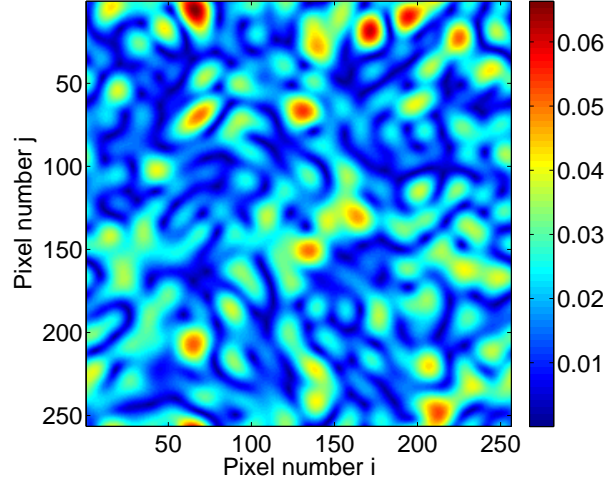


Fig. 1. Map of the square modulus of one scattering coefficient (arbitrary unit) generated by the sum of random phasors method.

spreads around the normal direction over a solid angle that roughly matches $(\lambda_0/\delta_x)^2$, with $\lambda_0 = \frac{2\pi c}{\omega_0}$ the central wavelength in air. The directions (k_x, k_y) are thus paraxial under condition $\delta_x \gg \lambda_0$ that is assumed thereafter. Spectrally, the scattered field is computed for N_f frequencies with a step $\delta_\nu = \frac{1}{N_f \delta_t}$. The frequencies are chosen to corresponds to $\nu_\ell = \nu_c + \ell \delta_\nu$ for $\ell \in [1 - N_f/2 : N_f/2]$ and ν_c an arbitrary central frequency. The simulated scattering coefficients vary in frequency with a chromatic length $\Delta\nu_\Sigma$:

$$\Delta\nu_\Sigma = \frac{1}{n_t \delta_t} \quad (5)$$

An example of the spectral variations of the scattering coefficients is provided in Fig. 2.

3. The polarization matrix

The polarization and coherence properties of time-stationary light is statistically characterized at first-order in the spectral domain by the so-called Wolf's spectral density matrix $\bar{\bar{W}}(\nu)$. This matrix is related to the harmonic decomposition (or generalized Fourier transform) of the fields by:

$$\langle \bar{\bar{e}}^*(\nu_1) \bar{\bar{e}}^\top(\nu_2) \rangle = \bar{\bar{W}}(\nu_2) \delta(\nu_2 - \nu_1) \quad (6)$$

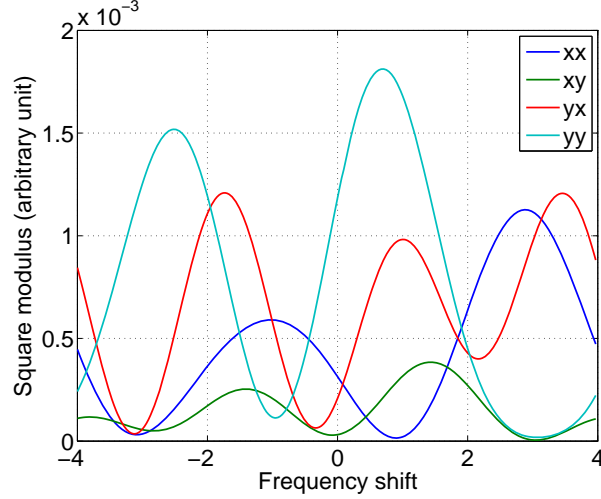


Fig. 2. Square modulus of the four scattering coefficients (arbitrary unit) generated by the spectral version of the sum of random phasors method in a given scattering direction against frequency (same unit as $\Delta\nu_{\Sigma}$).

denoting δ the Dirac distribution. With (2) and in the case of a deterministic scattering medium, scattered and incident spectral density matrices become directly connected :

$$\bar{\mathbb{W}}^s(\nu) = \bar{\Sigma}^*(\nu) \bar{\mathbb{W}}^i(\nu) \bar{\Sigma}^T(\nu) \quad (7)$$

so that the scattered field polarization state can be deduced from the incident field spectral density matrix and spectrally varying scattering matrix.

For both incident and scattered light, the polarization state is deduced from the spectral density matrix through the polarization matrix \bar{J} .

$$\bar{J} = \int_0^\infty \bar{\mathbb{W}}(\nu) d\nu = \frac{I}{2} \begin{bmatrix} 1 + P \cos 2\chi \cos 2\psi & P(\cos 2\chi \sin 2\psi + i \sin 2\chi) \\ P(\cos 2\chi \sin 2\psi - i \sin 2\chi) & 1 - P \cos 2\chi \cos 2\psi \end{bmatrix} \quad (8)$$

The polarization matrix is related to the optical intensity I and to the Poincaré sphere representation (P, ψ, χ) of the polarization state [28]. The DoP P varies from 0 for totally depolarized light such as natural light to 1 for totally polarized light. χ and ψ are the ellipticity and orientation angles, respectively.

4. Enpolarization

We start testing our model on a totally unpolarized incident light. In order to force $P_i = 0$, the incident spectral density matrix is set to the following expression:

$$\bar{\mathbb{W}}^i(\nu) = I_i \begin{bmatrix} 1 & 0 \\ 0 & 1 \end{bmatrix} \frac{e^{-2\pi((\nu-\nu_c)/\Delta\nu_i)^2}}{\sqrt{2}\Delta\nu_i} \quad (9)$$

This matrix is thus the simple product of a polarization matrix and a scalar function of frequency. This last function exhibits a Gaussian dependency on frequency, mimicking a Doppler-broadened source. Its central frequency is denoted ν_c and its spectral bandwidth $\Delta\nu_i$ follows one

of the classical definitions [29, eq. 4.3-83]. In optics, one can easily assume that bandwidth $\Delta\nu_i$ is much smaller than frequency ν_c .

The scattered field polarization matrix is now computed following formulas (7) and (8) with the scattering matrix detailed in section 2. The simulation results do not depend on the absolute value of the incident bandwidth $\Delta\nu_i$ or the chromatic length $\Delta\nu_\Sigma$ of the scattering coefficients, but on their dimensionless ratio R .

$$R = \frac{\Delta\nu_i}{\Delta\nu_\Sigma} \quad (10)$$

The scattered DoP, denoted P_s , is investigated for the ratio R varying between 1/10 and 10. Its probability density functions, or densities, are given in Fig. 3 for five values of R , and the

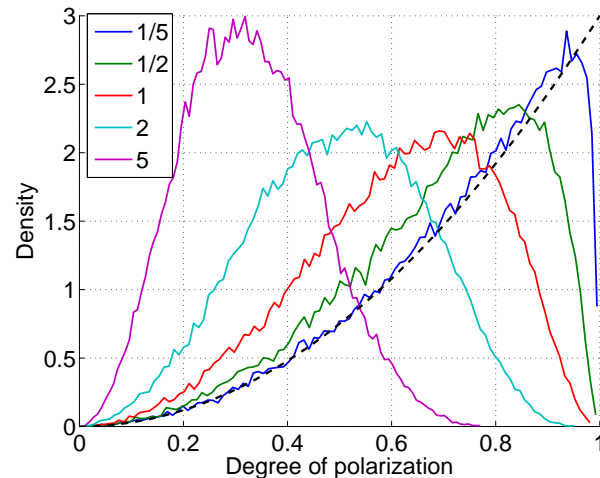


Fig. 3. Scattered DoP densities for unpolarized incident light and five different values of the incident bandwidth to scattering coefficients correlation length ratio R (solid lines) and the $3P_s^2$ density (dashed line).

mean scattered DoP is plotted against ratio R in Fig. 4 (blue curve). Enpolarization effect is quite impressive, with a mean scattered DoP scaling from 0.24 to 0.75 for the studied R ratio range. For small values of the R ratio, where spectral variations of the scattering coefficients are negligible, the classical density $3P_s^2$ for the scattered degree of polarization P_s [12] is retrieved. This density is plotted in Fig. 3 (dashed line) so that it can be compared to the density for $R = 1/5$ (blue curve). It is remarkable that the asymptotic density is followed as soon as $1/R = 5$. It is also worth to retain that when the spectral characteristics of incident light and scattering coefficients are close, typically around $R = 1$, the scattered DoP reaches 0.6 in average. To finish with unpolarized incident light, it appears on both Figs. 3 and 4 that the scattered DoP is globally shifted toward zero when the R ratio is raised. For $R = 5$, the scattered DoP density spreads between 0 and 0.8, with a mean value as low as 0.33. However, one can assume that this mean scattered DoP will go on decreasing with R increasing, with zero limit for infinite R ratio. This asymptotics is proving difficult to investigate numerically.

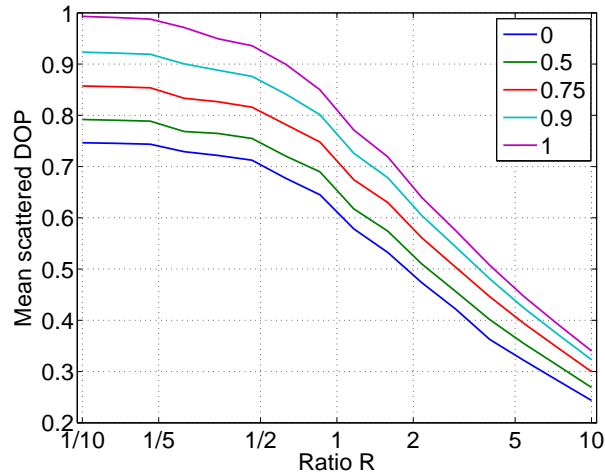


Fig. 4. Mean scattered DoP against the incident bandwidth to scattering coefficients correlation length ratio R for five different values of the incident DoP P_i .

5. Depolarization

We now move on to polarized incident light. The expression (9) of the incident spectral density matrix is directly generalized to nonzero values $P_i > 0$ of the incident DoP:

$$\bar{W}^i(\nu) = \bar{J}_i(P_i, \chi_i, \psi_i) \frac{e^{-2\pi((\nu-\nu_c)/\Delta\nu_i)^2}}{\sqrt{2}\Delta\nu_i} \quad (11)$$

In the strong scattering regime which is the context of our study and underlies our scattering coefficients simulations (section 2), the scattered light DoP can be expected to only depend on one incident light polarization parameter over three, namely the DoP P_i . This idea has been confirmed numerically: the incident light ellipticity χ_i and orientation ψ_i angles have no statistical influence on the DoP of the scattered light. This is the reason why no further details are given on the polarization matrix \bar{J}_i . Also, the polarimetric angles χ_s and ψ_s appear statistically independent of the incident polarization state and scattered DoP, and are distributed so that no direction in the Poincaré sphere is privileged.

The scattered DoP P_s is studied for totally polarized incident light by setting $P_i = 1$. The mean scattered DoP against the ratio R as defined in (10) is plotted in Fig. 4 (magenta curve), and the scattered DoP densities are given in Fig. 5. Again, it appears that light is more depolarized when the ratio R is higher. Depolarization makes the mean scattered DoP reach 0.99 for $R = 1/10$, 0.80 for $R = 1$ and 0.34 for $R = 10$. For large values of R , the scattered DoP densities are similar to the previous ones, presented in Fig. 3 and obtained for unpolarized incident light, even if centered on slightly higher levels. However, this similarity vanishes when R tends toward zero. The lowest DoP are more and more depopulated, with a density confined between 0.8 and 1 for $R = 1/5$. The density rather tends toward a Dirac function around $P_s = 1$. On Fig. 5, the density for $R = 1/5$ is truncated, since it reaches as high as 70 around $P_s = 1$.

Up to now, we consider only extreme degrees of polarization for incident light, so that only enpolarization or depolarization can occur, whatever the (finite) value of the incident bandwidth to scattering coefficients correlation length ratio R . At present, we study a scattering medium enlightened by an partially polarized field. The mean scattered DoP is plotted against ratio R

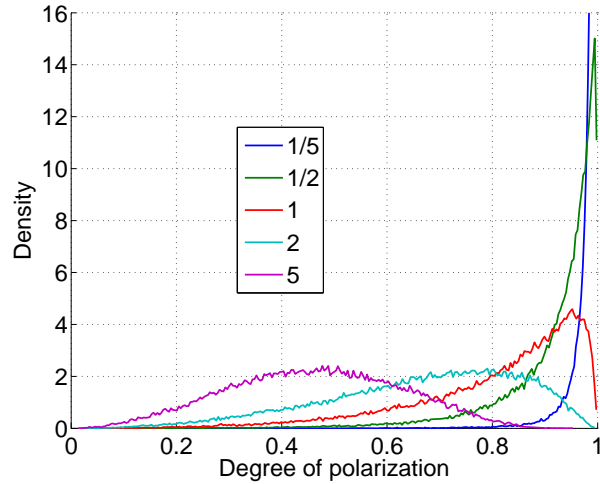


Fig. 5. Scattered DoP densities for fully polarized incident light and different values of the incident bandwidth to scattering coefficients chromatic length ratio R .

in Fig. 4 for three values of the incident DoP : 0.5 (green curve), 0.75 (red curve) and 0.9 (cyan curve). The $P_i = 0.25$ case reveals very close to the unpolarized case detailed in the previous section, the reason why it has not been included in Fig. 4. Moreover, it is systematically enpolarized for $1/10 \leq R \leq 10$. For $P_i = 0.5$ (green curve), enpolarization occurs for R ratios smaller than 2.3, while light is depolarized thereafter. We are thus able to estimate, for any incident DoP, the boundary value R_L of the ratio R between enpolarization and depolarization. For red and cyan curves of Fig. 4, we find $R_L = 0.84$ and $R_L = 0.25$, respectively. A more

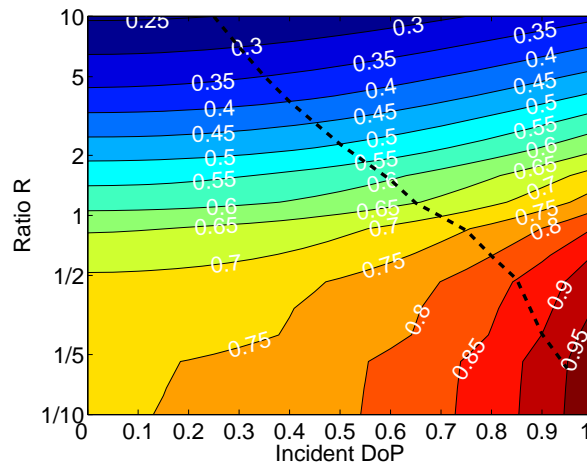


Fig. 6. Mean scattered DoP against the incident bandwidth to scattering coefficients chromatic length ratio R for different values of the incident DoP P_i .

methodical study of the mean scattered DoP with respect to the incident DoP and the incident bandwidth to scattering coefficients correlation length ratio R over the $[1/10; 10]$ range is given

in Fig. 6. This is a filled contour plot of the mean scattered DoP, with levels of the isolines in white and the black dashed curve representing R_L : below or to the left of this black dashed curve are the scattering events that corresponds to an enpolarization of light, while depolarization occurs above or to the right.

We now try to modelize the variations of R_L with P_i . For this, we have numerical data over the range $1/10 \leq R \leq 10$, and two asymptotic values: whatever the finite incident bandwidth to scattering coefficients correlation length ratio R , enpolarization occurs for totally unpolarized incident light and depolarization occurs for totally polarized light. We therefore have to meet the two following limits:

$$\lim_{P_i \rightarrow 0} R_L = +\infty \quad \lim_{P_i \rightarrow 1} R_L = 0 \quad (12)$$

We found by trial and error, and with no supplementary theoretical argument that the empirical model (13) was relevant, with linear regression leading to values $a = 0.7$ and $b = 0.0$.

$$R_L = au + b \quad u = \tanh^{-1}(1 - 2P_i^2) \quad (13)$$

On Fig. 7, the numerical data and the output of model (13) are plotted in blue.

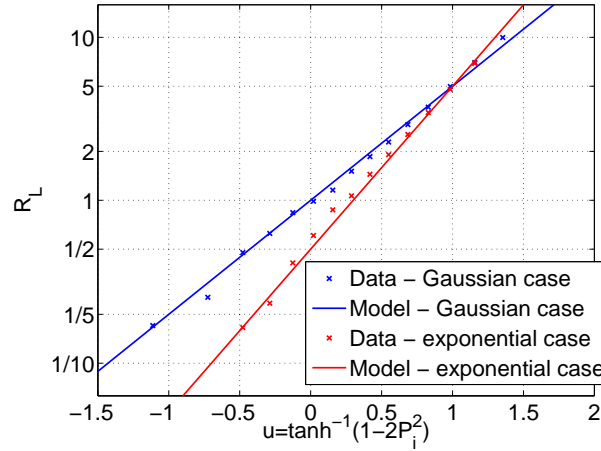


Fig. 7. R_L against $u = \tanh^{-1}(1 - 2P_i^2)$ with P_i the incident DoP for numerical data in the Gaussian correlation case (blue symbols), for model (13) with parameters $a = 0.7$ and $b = 0.0$ (blue line), for numerical data in the exponential correlation case (red symbols) and for model (13) with $a = 1.0$ and $b = -0.3$ (red line).

All previously presented results were obtained under the assumption that incident light was spectrally broad due to Doppler effect. Consequently, the spectral density matrices (9) and (11) were sharing Gaussian variations with frequency. Another classical kind of sources are collision-broadened, with a Lorentzian dependency on frequency. They are now briefly investigated, since phenomena and results are qualitatively close to the Gaussian case. The mean scattered DoP is plotted against the incident DoP and ratio R in Fig. 8. Once again, the black dashed curve corresponds to the values of R_L . This last quantity can still be modeled by (13), with this time parameters set to $a = 1.0$ and $b = -0.3$, as it appears on Fig. 7 (red symbols and red line).

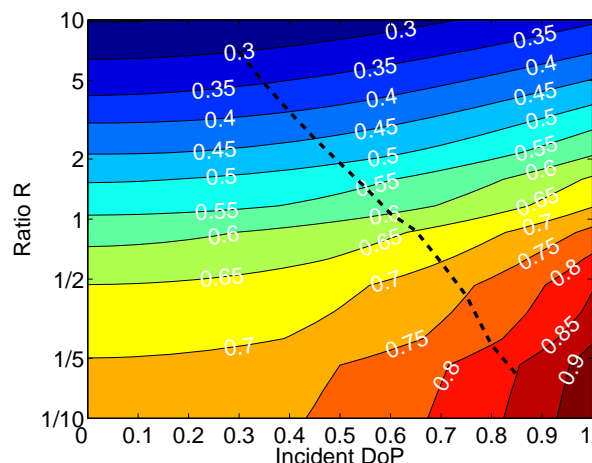


Fig. 8. Mean scattered DoP against the incident bandwidth to scattering coefficients chromatic length ratio R for different values of the incident DoP P_i in the case of a Lorentzian dependency to frequency.

6. Conclusion

In this paper, a theory was derived for the scattering of partially coherent and polarized light from a disordered medium with chromatic (wavelength-varying) scattering coefficients over the incident light bandwidth. With an extension of the empirical model of the random phasors, scattering matrices are generated that can simulate a large class of strong scattering events in Optics.

It is found that the incident light bandwidth over scattering coefficients spectral correlation length ratio R is the key parameter in this analysis. For values $1/5$, $1/2$, 1 , 2 , and 5 of this ratio, the scattered DOP distribution is estimated and plotted for both totally depolarized and totally polarized incident light. Then the mean scattered DoP is mapped as a function of both the ratio R ranging between $1/10$ and 10 and the incident light DoP. Both cases of Doppler-broadened and collision-broadened sources of light are investigated. Finally, this empirical model for the scattered DoP leads to a simple analytical formula for the value of the cut-off ratio against the incident DoP.

We now summarize some salient results of our analysis:

- repolarization of a totally depolarized light with a $3P_s^2$ law is almost retrieved as soon as the ratio R is smaller than $1/5$ (Doppler-broadened source),
- variations with wavelength of the scattering coefficients can explain local depolarization of a totally polarized light by deterministic media,
- a linear variation of the mean scattered DoP with $\tanh^{-1}(1 - 2P_i^2)$ is numerically shown.

We remind some assumptions that we made in the numerical sections of this paper in order to reduce the number of freedom degrees. The shape of the incident spectral density matrix has been forced as the product of a polarization matrix and a function of frequency. As a consequence, the four matrix elements share the same dependency to frequency. It also implies that the so-called spectral degree of coherence [5] is constant. We stress that our model can be applied to any arbitrary spectral density matrix.

Furthermore, with the random phasors empirical scattering model as we extend it, the scattering coefficients share the same spectral correlation length. This may be a too simplifying, unphysical assumption. We are currently working on rigorous electromagnetic scattering from rough surfaces and heterogeneous bulks models to provide more realistic scattering matrices. Finally, this theoretical and numerical work have to be confirmed by experimental data. A first step in this direction is to characterize chromatically some scattering samples, such as the Lambertian scattering standards already studied in [12, 20]. An optical set-up is currently being mounted with a wavelength-agile narrow linewidth source.

Acknowledgments

This work was performed in the TraMEL project thanks to the financial support of French National Research Agency (Project TraMEL # 10-BLAN-0315).